Crack-Size Effects on Cyclic and Monotonic Crack Growth in Polycrystalline Alumina: Quantification of the Role of Grain Bridging

J. J. Kruzic,* R. M. Cannon,** and R. O. Ritchie[†]

Materials Sciences Division, Lawrence Berkeley National Laboratory, and
Department of Materials Science and Engineering, University of California, Berkeley, California 94720

The role of grain bridging in affecting the initial rising portion of the *R*-curve and the transient, non-steady-state behavior of short cracks during (cyclic) fatigue-crack propagation has been *quantitatively* examined in a 99.5% pure alumina. Fatigue-crack growth properties for both long and short ($\Delta a_f < 2$ mm) cracks emanating from machined notches (root radius, $\rho \sim 15–150$ μm) were investigated, where Δa_f is the extension of the fatigue crack from the notch. Growth rates (da/dN) were far higher at the same applied stress-intensity range (ΔK) and fatigue thresholds, ΔK_{TH}, were markedly lower for short cracks than for corresponding long cracks. Crack extension was measured at the lowest driving forces for short cracks emanating from razor micronotches with $\rho \approx 15$ μm. For growth rates $<10^{-8}$ m/cycle, da/dN vs ΔK curves for short cracks merged with the demonstrably steady-state curve for long cracks after ~2 mm of crack extension. This length corresponds well to the extent of the measured crack-bridging zone for a near-threshold steady-state fatigue crack. For $da/dN > 10^{-8}$ m/cycle, however, non-steady-state behavior was observed at all crack sizes, indicating that achieving steady state at each ΔK level is difficult. The crack-tip shielding contribution due to such grain bridging was determined using both direct compliance and the more accurate multi-cutting/crack-opening profile techniques. Bridging stress-intensity factors were computed and subtracted from the applied stress intensities to estimate an effective (near-tip) driving force, ΔK_{eff}. These results provided (i) a lower threshold (in terms of ΔK_{eff}) below which both long and short fatigue cracks should not propagate, and (ii) an estimate of the intrinsic toughness, K_0, for the start of the *R*-curve. Such results quantitatively affirm that the reduced role of grain bridging is a primary source of the transient behavior of short cracks in grain-bridging alumina-based ceramics under cyclic loading.

I. Introduction

THE principle of similitude, which is implicit in linear-elastic fracture mechanics,[1–3] states that two cracks, regardless of their size, will behave in identical fashion provided they are subjected to the same stress intensity, *K*. Despite this notion, for the successful implementation of damage-tolerant design and life-prediction methodologies, it is necessary in many materials that the subcritical crack-growth and toughness properties of a structural material are determined for cracks of a size comparable to those encountered in service. This is important because, in reality, short cracks can behave quite differently from larger cracks, in particular by exhibiting rising fracture resistance with extension under monotonically increasing loading, i.e., *R*-curve behavior.[4–12] Although *R*-curve behavior has been extensively studied in ceramics,[4–12] it must be recognized that most published *R*-curves have measured initiation toughness values, K_0, several times larger than the single crystal toughness, an unreasonable situation for materials that fail intergranularly. Despite this fact, only a few studies have attempted to deduce a more accurate assessment of K_0,[13–15] with only one doing so by quantifying the role of grain bridging,[13] making this an ongoing area of investigation which is considered in the present paper.

A corollary for *R*-curve exhibiting materials is that the fatigue-crack growth rates for short cracks should far exceed those of corresponding large cracks subjected to the same applied driving force and they should propagate at applied ΔK levels *less than* the fatigue threshold, ΔK_{TH}, below which large cracks are presumed to be dormant.[3,16,17] Such crack size effects in fatigue are widely observed in metals and expected in ceramics where crack sizes are comparable to, or less than, one of three characteristic dimensions, namely, of the microstructure (microstructurally small), the extent of local inelasticity (plastic-zone size) *ahead* of the crack tip (mechanically short/small), and/or the extent of the zone causing crack-tip shielding or bridging *behind* the crack tip (functionally short/small).[3,17] Such cracks are denoted as short when they meet such conditions in only one dimension, i.e., the crack length, and small when one or more such conditions are met in all dimensions. A functionally short crack has limited crack-tip shielding, yet samples the microstructure statistically because of its extensive crack front.[16] In contrast, functionally small cracks are small in all dimensions, as typified by a small, semielliptical surface flaw. When small cracks are comparable in size to microstructural entities, in addition to reduced shielding, biased sampling of microstructurally weak paths may occur. Because of these restrictions in shielding and microstructural sampling, the crack-growth resistance of microstructurally small cracks often tends to be the lowest.

The problem of short or small flaws is especially a concern for ceramics, where due to their characteristically low toughness, large flaws cannot generally be tolerated. Consequently, in ceramics such as alumina, which derive their toughening from grain bridging in the crack wake, crack-size effects are particularly significant as critical crack sizes are often much smaller than the length of the steady-state bridging zones. Despite the importance of this topic, only a handful of studies have attempted to examine short or small crack effects in the cyclic fatigue of nontransforming, grain-bridging ceramics, with the majority of investigations focused on small surface cracks growing from hardness indentations.[18–25] Because crack sizes in many of these investigations were in fact large compared with grain-bridging zones, once the local residual stresses due to the indents were either taken into account in the calculation of the total driving force or removed by polishing, there was no obvious difference in crack-growth behavior over the range of crack sizes tested.[18–20,25] While several studies have reportedly observed short- and/or small-crack fatigue

effects thought to be attributable to limited crack-tip shielding,[22,23] evidence linking the two phenomena has been limited and ambiguous. Additionally, none of these studies have effectively quantified the crack shielding for long versus short cracks, which in turn would allow for the prediction of short-crack behavior.

Recent work by the authors has shown that for through-thickness fatigue cracks emanating from alumina/aluminum interfaces into the alumina, anomalous rapid crack-growth behavior similar to that of short cracks was seen for the initial ~2 mm of crack extension; thereafter, crack-growth rates were identical to those measured for long cracks in the alumina.[26] Owing to the large (millimeter dimension) bridging zones in this particular alumina, reduced crack-tip shielding from grain bridging was suspected as the cause of the initially faster growth rates. It was thus reasoned that this particular alumina would represent an ideal material with which to investigate crack-size effects in the fatigue of ceramics. Accordingly, the objectives of the present work are (i) to investigate the role of reduced grain bridging in the short-crack fatigue behavior of grain-bridging ceramics by using through-thickness cracks in this polycrystalline alumina, and (ii) to obtain *quantitative* measurements of the bridging contributions in this alumina, which can provide estimates for the worst case, i.e., lowest, fatigue threshold for which fatigue-crack propagation can occur in this material, as well as for the intrinsic toughness, or initiation point, on the *R*-curve.

II. Background

In grain-bridging ceramics, the driving force for crack growth (e.g., the stress intensity) experienced at the crack tip is lowered relative to the applied driving force due to forces acting in the crack wake. These forces are caused by intact elastic ligaments bridging the crack flanks as well as by frictional tractions that develop along the fractured grain boundaries during crack extension; such bridges sustain load and act to shield the crack tip from the applied loads.[5,8,27] These phenomena account for increasing crack-growth resistance with crack extension under monotonically increasing loading. Grain bridging has been found to exist in the crack wake over dimensions that are comparable with the amount of crack extension needed to reach the plateau of the rising *R*-curve, typically on the order of several hundred micrometers, but up to several millimeters for some alumina-based ceramics.[8,14,28] In bridging materials, the applied stress intensity, K_{app}, is equal to the sum of the bridging stress intensity, K_{br}, and the near-tip stress intensity, K_{tip}, and accordingly, K_{tip} may be expressed as

$$K_{tip} = K_{app} - K_{br} \qquad (1)$$

So defined, K_{br} is then the magnitude of stress intensity not directly experienced at the crack tip due to the load sustained by the bridges. Thus, if K_{br} is quantified, the initiation point on the *R*-curve may be deduced using Eq. (1) by noting that $K_0 = K_{tip}$ at initiation.

Cyclic fatigue effects in nontransforming, monolithic ceramics have in turn been attributed to a cyclic-loading induced degradation of bridging in the crack wake, which promotes crack advance by enhancing the near-tip driving force.[29–33] Under cyclic loading, such wake bridging is degraded by mechanisms such as frictional wear at the cracked grain boundaries or local chipping of bridging elements. It is thought that the intrinsic crack-advance mechanisms at or ahead of the crack tip, however, are unchanged from that under monotonic loading but may be aided by environmental interactions at the crack tip.[29–33] Thus, an effective (near-tip) stress-intensity range, ΔK_{eff}, may be defined for cyclic loading in the presence of bridging, in contrast to the applied driving force ΔK ($= K_{max} - K_{min}$). In this case, the peak bridging contribution, K_{br}, is subtracted from K_{max} such that

$$\Delta K_{eff} = (K_{max} - K_{br}) - K_{min} \qquad (2)$$

where K_{max} and K_{min} are the maximum and minimum applied stress intensities determined by the maximum and minimum

applied loads, P_{max} and P_{min}, for any given crack length. For tension–tension loading, the effects on K_{min} are comparatively small; thus the primary result of bridging in fatigue is a reduction in the maximum stress intensity experienced locally at the crack tip, leading to a reduction in ΔK_{eff}, and a corresponding decrease in the effective ratio of minimum to maximum driving force. As the value of K_{br} may be lower for short cracks than for long cracks because of an inherently shorter grain-bridging zone, ΔK_{eff} will be larger at a given applied ΔK level, leading to a higher growth rate.

It should be recognized, however, that the degradation of the bridging zone in fatigue almost certainly depends on ΔK; in addition, for a constant applied load ratio, $R = P_{min}/P_{max}$, ΔK also reflects the effect of K_{max} on crack growth. Thus, a unique steady-state crack-growth relation da/dN vs ΔK should exist for long cracks, for which the bridging zone is equilibrated at every ΔK. Additionally, a variety of transient situations exist, in principle, depending on loading history and crack length, giving rise to phenomena such as short-crack effects. From Eq. (2), it is seen that if the bridging stress intensity for long cracks is quantified, fatigue results may be presented in terms of ΔK_{eff}, thus providing a worst-case threshold for the fatigue behavior of cracks at all sizes; this is especially important for ceramics.

Several techniques exist for the estimation or quantification of K_{br}; however, these have rarely been applied to deduce intrinsic toughness values[13] or to understand short-crack fatigue phenomena in ceramics. One technique developed for estimating K_{br} in fiber-reinforced aluminum laminates compares the experimentally measured compliance of the bridged crack to the theoretical compliance for a traction-free crack of the same size,[34] as schematically illustrated in Fig. 1. In this context, and throughout this paper, the crack length, a, is measured with the crack tip defined to be at the farthest extent of detectable cracking from the loadline (i.e., all bridges are considered as part of the crack). This method allows for a determination of the additional load sustained at the load line, P_{br}, due to the presence of the bridges, which may be used to approximate K_{br} using standard stress-intensity solutions for the given geometry, i.e., $K_{br} = f(P_{br}, a)$. However, an accurate assessment involves the determination of the bridging stress distribution behind the crack tip, $\sigma_{br}(x)$, from which K_{br} may be calculated using[35,36]

$$K_{br} = \int_0^a h(x,a)\, \sigma_{br}(x)\, \mathrm{d}x \qquad (3)$$

where $h(x,a)$ is a geometry-dependent weight function, a is the crack length, and x is the position where the stress acts. Several methods for quantifying the bridging tractions behind the crack tip have been developed. One destructive technique uses a diamond saw blade to incrementally cut away the crack wake while measuring the sample compliance after each cut;[37–39] another
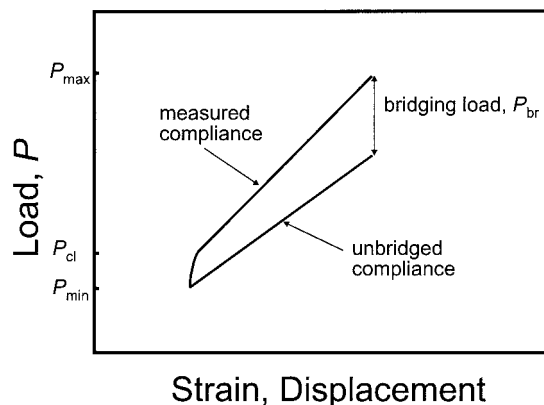

Fig. 1. Schematic illustration showing how the effective bridging load, P_{br}, is determined using measured and calculated compliance curves.[34] P_{br} is used to estimate the corresponding bridging stress intensity, K_{br}.

involves machining "postfracture tensile specimens" out of the bridged crack wake for subsequent tensile testing.[30,40,41] Conversely, one may determine bridging stresses nondestructively by measuring the crack-opening profile under load and comparing that to the computed traction-free opening, and then finding a $\sigma_{br}(x)$ that accounts for the difference.[14,15,42,43] In the present work, all but the postfracture tensile technique are used to quantify the role of grain bridging in the fracture and fatigue of short and long cracks in an alumina-based ceramic.

III. Procedures

(1) Material

The material investigated was Coors AD995 alumina (99.5% pure, ≥98% dense), which has a variable grain size ranging typically from ~1 to 50 μm. A mean linear intercept of 12 μm was obtained from 32 measurements on 3 micrographs, which corresponds to a nominal (average) grain size of $d_g \approx 18$ μm using ASTM Standard E112. To obtain an approximate grain size distribution, effective grain diameters, defined as the average of the long and short axes, were measured for all of the grains in the micrograph shown in the inset of Fig. 2. While the actual grain diameters are underestimated by this method since only a random slice through each grain is observed in the micrograph, it is expected that a reasonable, approximate grain size distribution may be obtained in this manner. Figure 2 presents the grain size distribution in terms of the percentage of total area of the micrograph occupied by the grains. Although most of the grains are in the 1–10 μm range, these grains in fact make up only a small fraction of the total material volume. Based on Fig. 2, the majority (~55%) of the material is made up from grains in the 15–35 μm range, with a significant volume fraction arising from even larger grains.

(2) Crack-Growth Experiments

As-received alumina blocks (21 mm square by 10 mm thick) were machined into 3 mm thick, compact-tension C(T) specimens; the nominal width W of these specimens was 17 mm. Except as noted, notches were diamond saw cut to an initial length of $a_0 \approx$ 4–5 mm, with notch root radii, ρ, ranging from 75 to 150 μm. Additional razor-micronotched samples ($\rho \approx 15$ μm) were made

for some tests, where the razor micronotch was created by repeatedly sliding a razor blade over the saw-cut notch in the presence of a 1 μm diamond slurry. All samples were lapped flat on both sides to a 1 μm finish using diamond polishing compounds so that cracks could be easily observed via optical and scanning electron microscopy. Fracture and fatigue tests were conducted in room air (25°C, 20–40% relative humidity) using computer-controlled servo-hydraulic testing machines. Sample compliance was measured using strain gauges mounted on the back face of the samples, and crack lengths were calculated using standard C(T) compliance calibrations.[44]

An R-curve was measured to evaluate the fracture resistance in terms of the stress intensity, K, under a monotonically increasing load as follows. Fatigue-precracked samples were loaded in displacement control until the onset of cracking, which was determined by a drop in load, at which point the sample was unloaded by ~10–20% of the peak load to record the sample compliance at the new crack length. This process was repeated episodically until termination of the test, at which point the compliance and loading data were analyzed to determine fracture resistance, K_R, as a function of crack extension, Δa. Because of crack bridging, errors invariably incurred in the compliance-crack length measurements; accordingly, renormalization to the actual crack length was achieved using optical microscopy, with the crack length, a, measured as previously defined. Discrepancies between the compliance and optically measured crack length were corrected by assuming that the error accumulated linearly with crack extension. Precracking was conducted by cycling the applied load until a fatigue crack emanated from a machined notch; to minimize the initial crack length, fatigue precracks were grown only to $\Delta a_f = 200$–300 μm before measurement of the R-curve, where Δa_f is the length of the fatigue crack extension from the machined notch, i.e., $\Delta a_f = a - a_0$.

Cyclic fatigue-crack growth rates for long cracks (provisionally defined and later justified as having $\Delta a_f > 2$ mm) were measured in general accordance with ASTM Standard E647. Tests were conducted at a frequency of 25 Hz (sine wave) using at a constant load ratio of $R = 0.1$. Crack lengths were continuously monitored and recorded at 20 μm increments on each sample using back-face strain compliance methods, again with periodic verification and correction from optical microscopy readings. A sample compliance curve may be seen in Fig. 3, where five consecutively measured compliance curves are plotted for a long crack fatigue
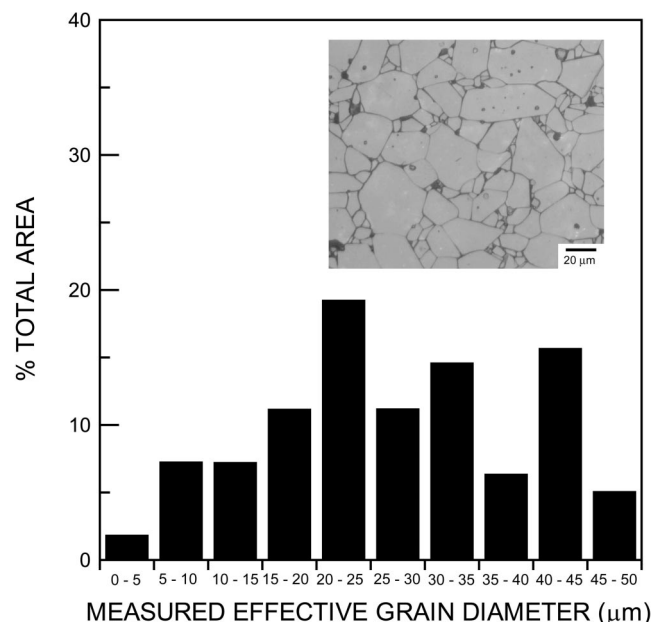

Fig. 2. Distributions of effective grain diameters presented in terms of percent total area based on the micrograph shown in the inset. The sample was thermally etched in air at 1550°C for 30 min.
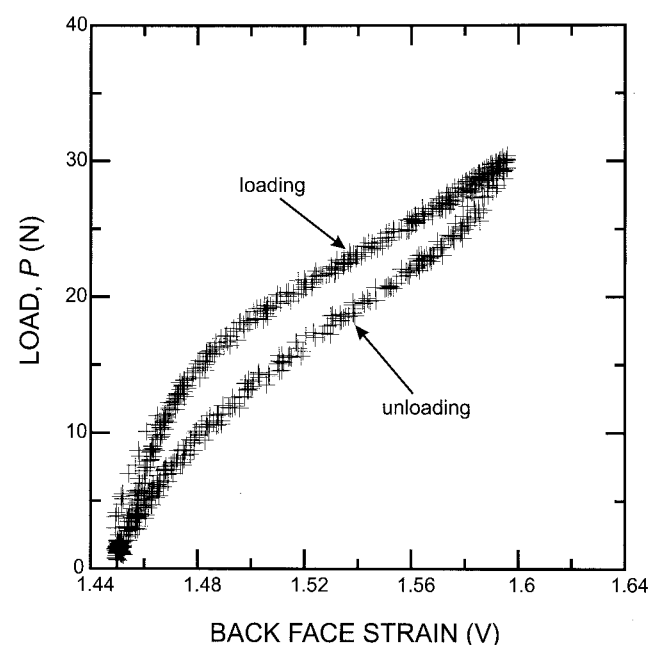

Fig. 3. Typical compliance curve for a long fatigue crack in AD995 alumina. Data represent five consecutive loading and unloading cycles.

specimen. It is apparent that there is considerable hysteresis in the compliance curve due to bridging. Accordingly, compliance measurements were taken as the slope of the linear portion of an unloading curve, while the nonlinear ends of the curve were ignored. Unless noted, growth rates, da/dN, were computed by averaging over a crack-growth range of ~ 100 μm and were characterized in terms of the stress-intensity range ΔK.

To find the steady-state behavior, crack-growth rates were measured under both increasing and decreasing ΔK conditions; the later method was used to obtain ΔK_{TH} fatigue thresholds, which were operationally defined as the minimum applied ΔK corresponding to growth rates below $\sim 10^{-10}$ m/cycle. Specifically, cracking was initiated by cycling until stable fatigue cracks formed ahead of the machined notches. After >2 mm of crack growth, the loads were either incrementally reduced to measure behavior approaching the steady-state threshold or increased to obtain the higher velocity portion of the crack-growth curves. Unless noted, continuous load adjustment was used to maintain a ΔK-gradient ($= (1/\Delta K)[d\Delta K/da]$) that was roughly constant at a value of ± 0.08 mm^{-1} within the limits of the accuracy of the compliance measurements of crack length. Ideally, this rate of change in ΔK would be sufficiently slow to allow the crack-bridging levels to adjust to the current ΔK level; however, due to the large, millimeter scale, bridging zones for AD995 alumina, this may not be possible, especially over the high velocity portion of the da/dN–ΔK curve. To test this, some experiments were conducted using lower ΔK-gradient values.

Corresponding fatigue-crack growth rates for short cracks, where $\Delta a_f < 2$ mm, were conducted on alumina samples using the same general procedures, although data were now recorded, under both increasing and decreasing ΔK conditions, for the first ~ 2 mm of crack growth for cracks initiated from the standard saw-cut notches; the $\Delta a_f < 2$ mm cutoff for short cracks represents the approximate crack length where non-steady-state growth rates were no longer observed. For the initial growth of a short crack emanating from a notch, the stress intensity may be written[45]

$$K = 1.12 k_t \sigma \sqrt{\pi \Delta a_f} \qquad (4)$$

where k_t is the stress-concentration factor for the notch and σ is the nominal applied stress. For the present geometry, Eq. (4) dominates only over a distance of $< \rho/6$ ahead of the notch, while for much longer extension, the standard C(T) stress-intensity expression becomes reasonably accurate. Furthermore, after the crack extends a distance $\geq \rho$, the effects of the finite notch width have diminished.[46] For short-crack fatigue tests in the present study, data collection did not usually begin until after 100 μm of crack growth in an attempt to allow for a continuous crack front to form along the thickness of the notch. Since 100 μm corresponds to $2\rho/3$ for the largest notches, stress-intensity corrections due to the presence of the notch were deemed to be unnecessary. With razor-micronotched specimens, data were collected after smaller extensions.

(3) Quantification of Bridging: Direct Compliance (DC) Method

As described above, estimates of the bridging load experienced at the load line were made at various points on the da/dN curve using the method shown in Fig. 1.[34] This involved periodically interrupting a long-crack fatigue test and measuring the sample compliance together with a direct optical measurement of the actual crack length. The measured crack length was then used to compute the theoretical compliance, using standard C(T) compliance calibrations,[44] which was then compared with the measured compliance of the sample to determine P_{br} (Fig. 1).

(4) Quantification of Bridging: Multi-Cutting/Crack-Opening Profile (MC/COP) Method

As described below, crack-opening profile measurements were made, and those results were used along with the results of

multi-cutting compliance experiments to obtain an estimate of the full bridging stress distribution.

(A) Crack Profile and Bridging-Zone Measurements: Crack-opening profile measurements were obtained by observing two cracked samples ($a \approx 14$ mm) loaded *in situ* in a field-emission scanning electron microscope (FESEM). For sample I, the crack was propagated by cyclic fatigue such that the last >3 mm of growth was conducted in the near-threshold growth regime ($da/dN < 7 \times 10^{-10}$ m/cycle). Conversely, the crack in sample II was propagated under monotonically increasing loading during *R*-curve testing. To ensure crack propagation did not occur during the *in situ* loading experiment, in each case the sample was loaded to a driving force of $K = 3.0$ MPa·m$^{1/2}$, which is roughly 10–20% less than the measured K_{max} at the long-crack fatigue threshold in this material. The crack lengths were checked in the FESEM to verify that crack propagation had not occurred during loading. The tortuous nature of the crack path resulted in some scatter in the measured crack openings; thus, measurements were made at 50 μm increments behind the crack tip to provide enough data points (>150) to obtain a reasonable assessment of the average crack-opening behavior. Measurements of the full crack opening, $2u_{tot}$, were made to a resolution of ~ 10 nm in the near-tip region using a magnification of 30,000$\times$. Specimens were coated with ~ 20 nm of gold to avoid charging; however, this thin coating was not expected to affect the crack opening measurements.

After crack-opening profiles were measured, the extent of the bridging zone behind the crack tip, L, was assessed on the same two samples using a multi-cutting compliance technique similar to that of Wittmann and Hu.[37–39] Specifically, a diamond saw blade was used to cut out the crack and incrementally eliminate the crack wake while the sample compliance, C_u, was measured via back-face strain gauges after each incremental saw cut. When the portion of crack wake eliminated is traction free, there is no change in compliance after cutting; however, if active bridges are eliminated from the crack wake by the saw blade, a corresponding increase in the sample compliance is expected. Thus, the extent of the grain-bridging zone behind the crack tip may be determined by observing the notch length where the compliance begins to increase during the multi-cutting experiment.

Additionally, the normalized grain-bridging stress distribution, $\sigma_{br}(x)/\sigma_{max}$, may be computed from the multi-cutting compliance data. In cases where the bridging-zone length is appreciably smaller than the sample size, it has been shown that during multi-cutting[37]

$$\frac{\sigma_{br}(x)}{\sigma_{max}} = -\frac{C^2(a)\, C_u'(x)}{C'(a)\, C_u^2(x)} \qquad (5)$$

where $C(a)$ is the traction-free compliance, $C_u(x)$ is the observed compliance after cutting to the position x measured from the load line, and $C'(z) = dC(z)/dz$. The grain-bridging stress distribution obtained from the multi-cutting compliance data is normalized by the factor σ_{max}, which corresponds to the maximum bridging stress at the crack tip. Using the normalized bridging stress distribution obtained from Eq. (5), σ_{max} may be determined from the measured crack-opening profile, as described below.

(B) Calculation of Bridging Stresses: A general procedure for computing the bridging stress distribution from measured crack-opening displacements has been outlined by Fett *et al.*[15] and is briefly presented here. The bridging stress distribution, σ_{br}, may be computed from the measured crack-opening displacements, u_{tot}, by solving the double integral equation:[15]

$$\frac{1}{E'} \int_0^a \int_{\max(x,x')}^a h(a',x)\, h(a',x')\, \sigma_{br}(x')\, da'\, dx' = u_{tot} - u_{app} \qquad (6)$$

where E' is Young's modulus (E in plane stress, $E/(1 - \nu^2)$ in plane strain, where ν is Poisson's ratio), and x is the position of interest with origin at the load line. The weight function, h, is geometry specific and has been derived for the C(T) specimen as[36]

$$h = \sqrt{\frac{2}{\pi a}}\, \frac{1}{\sqrt{1 - x/a}} \left[1 + \sum_{(v,\mu)} \frac{A_{v\mu}(a/W)^{\mu}}{(1 - a/W)^{3/2}} (1 - x/a)^{v+1} \right]$$

$$(7)$$

where the coefficients $A_{v\mu}$ may be found in Ref. 36. The displacements due to the applied loading, u_{app}, for an unbridged crack at a given applied stress intensity, K_{app}, may be calculated as[47]

$$u_{app} = \frac{1}{E'} \int_{x}^{a} K_{app}(a')\, h(a',x)\, da'$$

$$(8)$$

For cases where the grain-bridging stress distribution could be determined from the multi-cutting experiments described above, the normalized stress distribution from Eq. (5) was substituted into Eq. (6) which was then solved; σ_{max} was determined from a least-squares fit to the experimental data. Where Eq. (5) was not valid (i.e., when $L \sim a$), to facilitate the solution of Eq. (6), a widely used strain softening form of the bridging stress distribution was chosen a priori:[8,28,40,42,48–51]

$$\sigma_{br} = \sigma_{max}\left(1 - \frac{X}{L}\right)^{n}$$

$$(9)$$

where X is the distance behind the crack tip ($X = a - x$), and L is the bridging-zone length. As L may be determined from the multi-cutting experiments, combining Eqs. (6) and (9) results in two unknown parameters remaining to be fit to the experimental data: σ_{max}, the maximum value of the bridging stress; and n, which describes the shape of the bridging stress distribution as it decreases from σ_{max} at the crack tip to zero at $X = L$. Such a function should provide adequate flexibility even when the bridging zone is not saturated since $n < 1$ gives functions with significant bridging stresses near the machined notch, as might be the case for a developing bridging zone. The optimal values of σ_{max} and n were chosen as those that gave a crack-opening profile nearest that measured experimentally, as determined by the least-squares method. Finally, values for the modulus and Poisson's ratio of the AD995 alumina were supplied by the manufacturer as $E = 372$ GPa and $v = 0.22$.

IV. Results

(1) Resistance-Curve Behavior

Measured R-curve data for the AD995 alumina are shown in Fig. 4. An initial toughness of $K_i \sim 3$ MPa·m$^{1/2}$ was measured at crack initiation from a 230 μm long fatigue precrack emanating from the machined notch. With further growth, rising R-curve behavior was observed after crack extensions as large as 8 mm with toughness values exceeding 6 MPa·m$^{1/2}$ (Fig. 4). Because of the small specimen size ($W \approx 17$ mm) and large bridging-zone length (>8 mm) for this alumina, a steady-state (plateau) toughness could not be obtained. Such large bridging zones under monotonic loading are consistent with results from other studies using aluminas with similar microstructure, where rising R-curves are observed after comparable crack extension.[4,6,41]

(2) Short- versus Long-Crack Fatigue Behavior

Both long ($\Delta a_f > 2$ mm) and short ($\Delta a_f < 2$ mm) fatigue-crack growth rates for AD995 alumina are presented in Figs. 5 and 6, respectively, as functions of the applied stress-intensity range, ΔK. The long-crack results (measured on several specimens using the standard tests described in Section III(2)), shown as the hatched region in Fig. 5, display characteristic Paris-power law behavior, i.e., $da/dN \propto \Delta K^m$.

To investigate the effect of the ΔK-gradient on the fatigue results, an additional long-crack fatigue experiment with increasing ΔK was conducted using lower K-gradient values than the standard 0.08 mm^{-1}. This allowed for ΔK to increase more slowly, with more crack growth occurring at each ΔK value, possibly
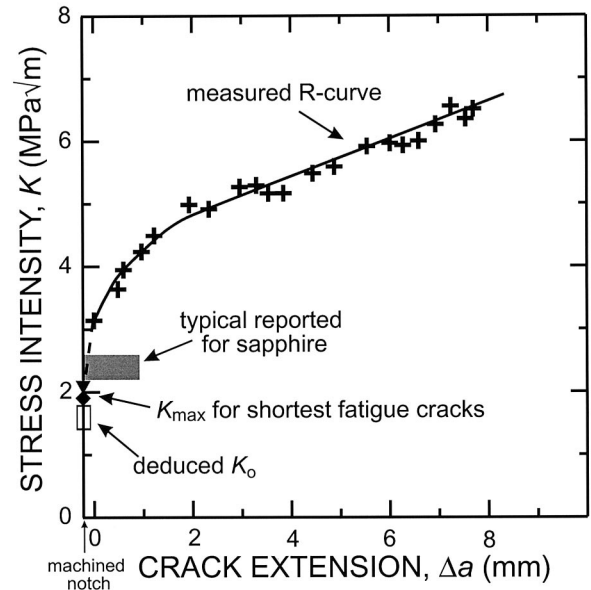

Fig. 4. *R*-curve measured for AD995 alumina demonstrating rising crack-growth resistance with crack extension. Data were collected from a fatigue precrack grown only 230 μm from the machined notch. Additionally shown are estimates for the initiation point of the *R*-curve based on the deduced intrinsic toughness, K_0, and the initial crack growth from razor micronotched specimens under cyclic loads. Typical values for sapphire fracture are shown for reference.

allowing for the development of longer cyclic grain-bridging zones and significantly different crack-growth behavior. Because of experimental difficulties, the ΔK-gradient was not held constant, but ranged between 0.025 and 0.08 mm^{-1}, with the highest values of the K-gradient corresponding to the highest values of ΔK. Additionally, because of erratic growth behavior at high driving forces, growth rates measured during this experiment were computed by averaging over 300 μm of crack growth; da/dN–ΔK data
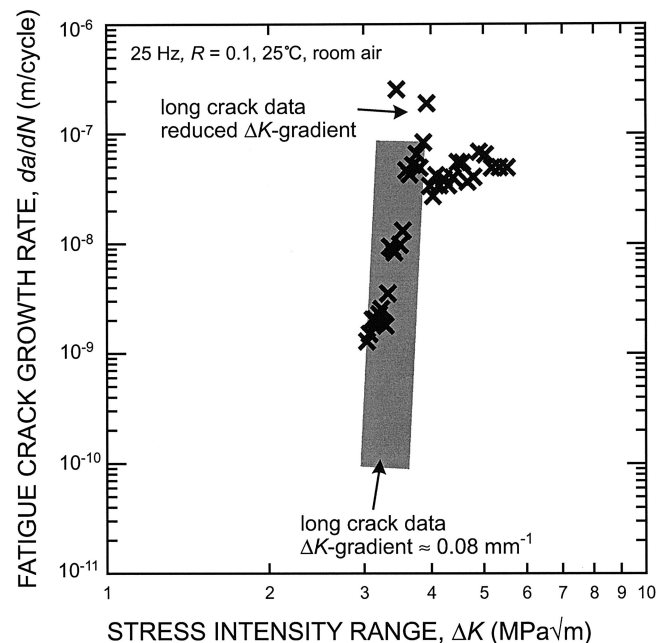

Fig. 5. Long-crack fatigue behavior of AD995 alumina shows the effects of using a lower ΔK-gradient. Below $\sim 10^{-8}$ m/cycle, the results appear insensitive to the ΔK-gradients used; at higher growth rates, distinctly different behavior is observed when the ΔK-gradient is reduced from the standard value.
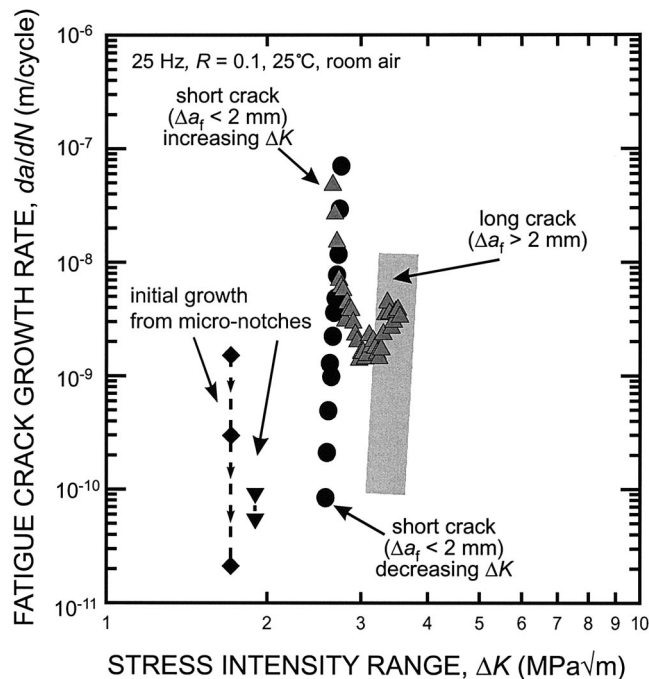
Fig. 6. Short-crack fatigue results for AD995 alumina. Using a standard notch, under decreasing ΔK conditions, a lower fatigue threshold is measured than for long cracks, while for increasing ΔK conditions, a V-shaped curve is observed, with data merging after ~2 mm of growth. Data also show the initial short-crack growth from razor micronotched specimens.

points for this test are shown in Fig. 5. For $da/dN < 10^{-8}$ m/cycle, the results are similar to the long-crack results where the ΔK-gradient was 0.08 mm^{-1}, indicating that for this growth-rate range a ΔK-gradient of 0.08 mm^{-1} is sufficiently low to allow for the bridging zone to adjust to each load level. Above 10^{-8} m/cycle, however, the results differ significantly, with stable crack growth occurring at higher ΔK values for the sample tested using a lower ΔK-gradient. Under these test conditions, the lower rate of increasing ΔK presumably allows for a much larger bridging zone to develop, with stable fatigue-crack growth occurring at ever higher points on the R-curve (Fig. 4). It is concluded that the long-crack fatigue results presented for growth rates below ~10^{-8} m/cycle using a ΔK-gradient of 0.08 mm^{-1} (the primary focus of this paper) represent conditions with an essentially steady-state bridging zone at each load level, while the conditions giving steady-state fatigue behavior at higher growth rates must be left for future investigations.

In contrast to long-crack results, short cracks demonstrated quite different behavior. For tests using the standard saw-cut notches with data taken after $\Delta a_f = 100$ μm:

(1) Under decreasing ΔK conditions, growth rates exhibited a similar power-law dependence on the applied ΔK level; however, the growth-rate curve, and hence ΔK_{TH} threshold, were displaced to values 15–25% lower than for corresponding long cracks.

(2) Under increasing ΔK conditions, growth rates initially *decreased* before finally increasing, at which point the da/dN–ΔK curve merged with that for long cracks. This behavior, which is characteristic of short fatigue cracks in metallic materials,[3,17] resulted in a V-shaped da/dN–ΔK curve (Fig. 6); short- and long-crack curves merged after ~2 mm of growth.

To determine whether short cracks may grow at driving forces below those measured using the standard notch for short-crack tests, additional experiments were conducted. For two specimens, a razor micronotch with root radius $\rho \approx 15$ μm was emplaced at the end of the saw-cut notch with three purposes: (1) to promote crack initiation at lower loads, (2) to reduce the distance over which notch effects on the stress intensity would be felt to only a few micrometers, and (3) to promote more uniform crack initiation

through the sample thickness. On cycling, it was observed that after crack initiation, growth occurred at applied driving forces of $\Delta K = 1.7$ and 1.9 MPa·m$^{1/2}$ in the two cases; when the cracks reached an average crack length of ~60 μm (as detected by compliance measurements) both cracks had essentially arrested. These results are presented in Fig. 6, with each data point representing ~20 μm of average crack growth (as measured by compliance).

(3) Crack Trajectories

FESEM analysis of cyclic and monotonic fracture surfaces indicated that failure occurred by predominantly intergranular fracture. Direct evidence of both uncracked ligament and frictional grain bridging in the crack wake is shown in Fig. 7. Similar bridges were observed for monotonically increasing and cyclic fatigue loaded samples; however, such bridges persisted much farther behind the crack tip for the case of the monotonically loaded sample.

(4) Crack Profile and Bridging Stress Distribution Results

Figure 8 shows the measured crack-opening profiles at a loading of $K_{app} = 3.0$ MPa·m$^{1/2}$ for both a near-threshold fatigue crack as well as a monotonically loaded crack previously loaded to higher levels during R-curve measurements. Also shown is the crack-opening profile for a traction-free crack computed using Eq. (8). It is apparent from Fig. 8 that both samples have crack openings smaller than the computed traction-free opening, with the monotonically loaded sample demonstrating the larger deviation
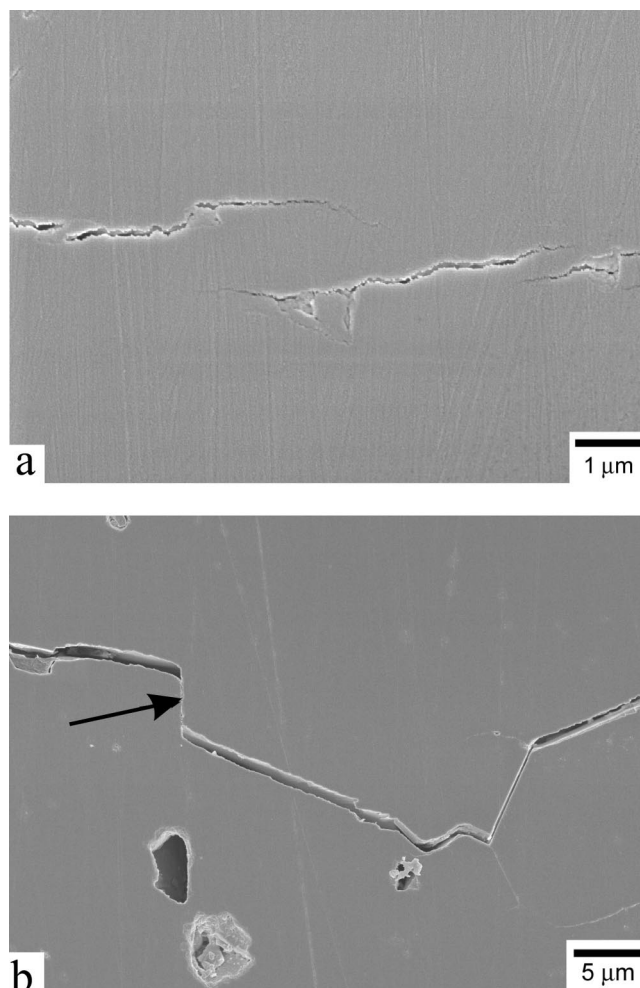

Fig. 7. (a) Elastic and (b) frictional grain bridging for *in situ* loaded cracks ($K = 3.0$ MPa·m$^{1/2}$); the arrow in (b) indicates the point of frictional contact. Crack propagation was from left to right.
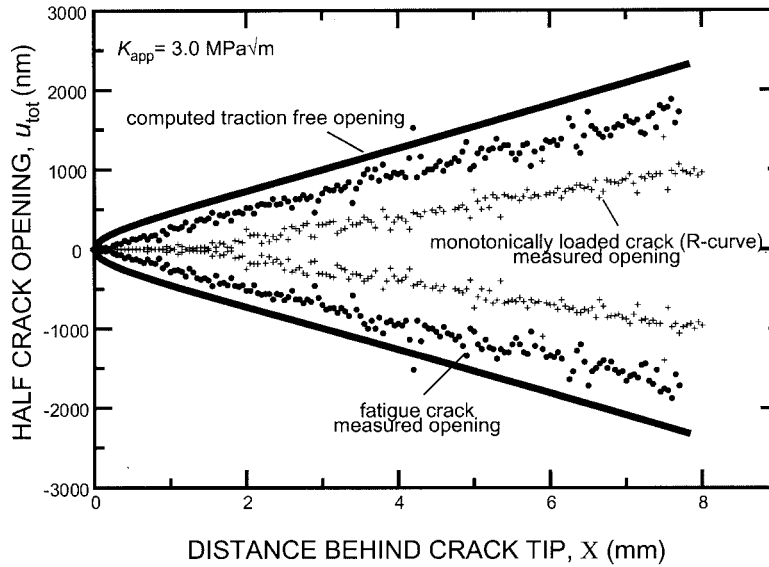
Fig. 8. Crack-opening profiles for both a near-threshold long fatigue crack and a monotonically loaded crack measured during *in situ* loading in an FESEM. The computed traction-free crack opening is also shown.

from traction-free behavior; indeed, at $K_{app} = 3$ MPa·m$^{1/2}$ the monotonically loaded crack remains essentially closed for ~1.5 mm behind the crack tip.

The results of the multi-cutting compliance experiments for each of these samples are shown in Fig. 9; each data point indicates an individual compliance measurement while the lines indicate best-fit polynomial functions to the data. Figure 9 shows that for the near-threshold steady-state fatigue crack, no increase in the sample compliance was observed during removal of the crack wake until the saw-cut notch reached within ~2 mm of the crack tip. This indicates a bridging-zone length of $L \approx 2$ mm for the near-threshold cyclic fatigue crack. Conversely, for the monotonically loaded sample, significant increases in compliance were

measured immediately after the starter notch was extended from its initial position (Fig. 9), thus indicating that the bridging zone extended the full length of the crack (i.e., $L = a - a_0$).

Using the above results, bridging-stress distributions, $\sigma_{br}(X)$, were calculated for both cases and are plotted in Fig. 10. For the fatigue crack, the normalized distribution $\sigma_{br}(X)/\sigma_{max}$ was computed directly from the best-fit of the results in Fig. 9 using Eq. (5);
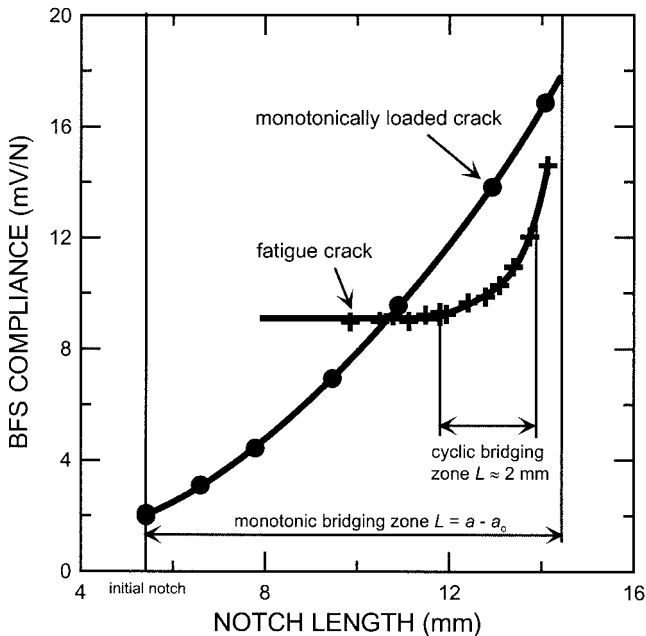

Fig. 9. Results from multi-cutting compliance experiments on a near-threshold long fatigue crack and a monotonically loaded crack demonstrating the difference in bridging-zone length. The indicated locations of the crack tip were measured by optical microscopy while each plotted data point corresponds to an individual compliance measurement.
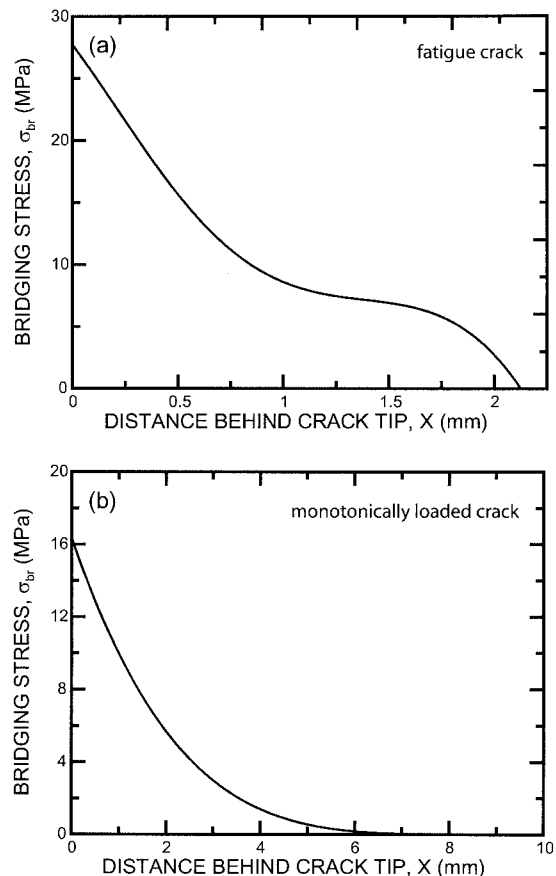

Fig. 10. Computed grain-bridging stress distributions for (a) a near-threshold long fatigue crack, and (b) a monotonically loaded crack.

the constant σ_{max} was determined to be 28 MPa from the crack-opening data. Because of the large extent of the grain-bridging zone for the monotonically loaded (R-curve) crack (Fig. 9), Eq. (5) could not be used to determine the grain-bridging stress distribution; instead a distribution of the form in Eq. (11) was assumed. For this sample, σ_{max} was computed to be 17 MPa, with an exponent of $n = 4.3$, indicating that bridging stresses have decayed to quite small values near the machined notch.

V. Discussion

(1) Quantification of K_{br}

Figure 10 shows the estimated grain-bridging stress distributions for both the near-threshold fatigue crack and the monotonically loaded crack. Although the fatigue crack experienced less shielding due to bridging, it exhibits a higher maximum bridging stress, σ_{max}, than the monotonically loaded crack in Fig. 10. It is important to note, however, that the fatigue crack was loaded to 80–90% of the load needed for crack extension, while the monotonically loaded sample was only loaded to <50% that needed for further growth for occur, thus accounting for the much lower maximum bridging stress for the monotonically loaded case. To confirm that the grain-bridging stress distribution estimates are reasonable, the bridging stress intensity, K_{br}, may be computed for each case using Eq. (3) and compared with expected values. Values of $K_{br} = 1.8$ and 2.8 MPa·m$^{1/2}$ were computed for the near-threshold fatigue crack and monotonically loaded crack, respectively. For the monotonically loaded crack, it is apparent from the opening profile in Fig. 8 that the crack is essentially closed until about 1.5 mm behind the crack tip; accordingly, the near-tip stress intensity, K_{tip}, is expected to be zero. Calculating K_{tip} using Eq. (1) yields a value of 0.2 MPa·m$^{1/2}$, or nearly zero, as expected.

(2) Completing the R-Curve

For the fatigue crack, K_{tip} is computed to be 1.2 MPa·m$^{1/2}$. To assess the plausibility of this value, first it may be assumed that crack advance occurs when

$$K_{tip} \geq K_0 \qquad (10)$$

where K_0 is the intrinsic stress intensity required for crack advance. At the fatigue threshold, it is assumed that the condition in Eq. (10) is met at the peak of the loading cycle, i.e., when $K_{max,tip} = K_0$. For the present fatigue crack, the applied loading corresponds to a level roughly 10–20% below the value of K_{max} at the fatigue threshold; thus, this estimated value of K_{tip} should give a lower bound to the actual value of K_0. Based on this result, an estimated range may be placed on K_0 by assuming the remaining 10–20% of stress intensity necessary for crack advance is added to the computed value of K_{tip} in the following ways:

(1) Assume the remaining additional 10–20% load raises K_{tip} and K_{br} proportionally, thus giving $K_0 = 1.4$–1.5 MPa·m$^{1/2}$.

(2) Assume K_{br} is saturated and the remaining additional 10–20% load raises only K_{tip}, giving $K_0 = 1.5$–1.8 MPa·m$^{1/2}$ (i.e., an upper-bound estimate).

Combining these ranges gives an estimate for the intrinsic toughness K_0 to be 1.6 ± 0.2 MPa·m$^{1/2}$; this range is plotted on the R-curve in Fig. 4 along with the estimated initial rising portion of the R-curve.

It is expected that K_0 should correspond nearly with the grain-boundary toughness for alumina, and accordingly be lower than that found for alumina single crystals (sapphire), since failure occurs primarily intergranularly. Various crystallographic planes of sapphire have been reported to have fracture energies, G_c, ranging from 12 to 17 J/m^2, except when near (0001), which does not crack.[52–55] Applying $K = (GE')^{1/2}$ gives a range of $K_c \approx$ 2.2–2.6 MPa·m$^{1/2}$, as shown in Fig. 4. Note, K_c for even the weakest sapphire planes exceeds the deduced K_0 as expected on physical grounds, and thus the deduced values of K_0, and correspondingly K_{br}, appear to be reasonable. Thus, the fracture energy

of the grain boundaries in the humid air environment may be as low as half that of sapphire at criticality, not unreasonable considering that Auger electron spectroscopy studies (see Ref. 56) revealed Ca at the grain boundaries which may lower the boundary toughness. One study[13] which quantified the role of bridging to deduce values of K_0 yielded ~2.0–2.3 MPa·m$^{1/2}$ for somewhat purer alumina. Other estimates of K_0 have been made for alumina from crack-opening profiles obtained after monotonic loading by fitting only the near-tip crack-opening region (assumed to be ahead of all the active bridging) to Irwin's traction-free parabolic elastic crack-opening profile. These studies yielded results in the 2.0–2.3 MPa·m$^{1/2}$ range[14,15] for the same aluminas as in Ref. 13; however, the present method and that used in Ref. 13 are considered more accurate since they take into account the entire crack-opening profile and explicitly quantify the effects of bridging. Indeed, fitting the crack-tip opening profile to a parabolic relation was unsuitable in the present study because the crack-opening profile in Fig. 8 is linear.

Additional measured estimates for K_0 are also shown in Fig. 4 based on K_{max} at the fatigue threshold for the shortest (~60 μm) cracks grown from micronotches. While these values are high because of some bridging present for these cracks, they do provide an improved estimate over that obtained from the traditional R-curve measurements; i.e., they fall below the sapphire toughness. Thus, cyclic precracking from very sharp notches can give improved estimates of the fracture resistance for very short cracks; however, fully quantifying and accounting for bridging, as described above, gives a more conservative, and reasonable, value of the crack-initiation toughness, K_0.

(3) Short- versus Long-Crack Cyclic Bridging Zones

In fatigue, it has been postulated that the extent of the steady-state, cyclic grain-bridging zone should correspond with the amount of growth necessary for short- and long-crack fatigue growth rates to merge.[26] This corresponds to the length of the initially short crack where its growth rates (under increasing ΔK conditions) are identical to those of a corresponding large crack at the same applied ΔK, implying that the grain-bridging zone has reached an equivalent, steady-state length for both cracks. The present results indicate that this is indeed the case for AD995 alumina, where the measured near-threshold cyclic grain-bridging zone length of 2 mm from Fig. 9 agrees well with the convergence point of the long- and short-crack fatigue data in Fig. 6. Additionally, this result agrees with estimates of the cyclic bridging-zone length from a previous study[26] based on crack extension needed to achieve steady state after long cracks at Al/Al$_2$O$_3$ interfaces deflected into the alumina. It is important to note, however, that the steady-state, cyclic grain-bridging zone length is not expected to be invariant for all crack-growth conditions; i.e., for higher growth rates the zone should approach that of a monotonically loaded crack. Experimental results using lower ΔK-gradients (Fig. 5) support this notion. For the present testing conditions, however, it was found that the convergence point of the short- and long-crack data for various samples occurred at growth rates between 3×10^{-10} and 1.5×10^{-9} m/cycle, i.e., similar to the growth rate range of the fatigue sample used for the multi-cutting experiment. Thus, it is expected that the cyclic grain-bridging zone length measured in Fig. 9 typifies both that of a near-threshold long crack as well as the short cracks in this study as they just reach steady state.

Additionally, using the results in Fig. 8 for the opening of a fatigue crack loaded to $K = 3.0$ MPa·m$^{1/2}$ (i.e., at ~10–20% below K_{max} at the fatigue threshold), a lower bound of $d_g/18$ may be placed on the critical crack opening above which active grain bridges no longer operate under near-threshold cyclic loading. This measured lower bound agrees favorably with previous estimates of the critical fatigue crack opening of $d_g/16$ for this alumina,[26] although no direct crack-opening measurements were made in that study. As expected, the critical crack opening in fatigue is well below the monotonically loaded critical crack openings of $d_g/4$ to

$d_g/3$ typically found in alumina[6,40] due to the degradation of bridging that occurs under cyclic loading conditions.

(4) Contribution of Grain Bridging for Fatigue

Figure 6 clearly demonstrates short-crack effects in AD995 alumina in the form of faster growth rates lower ΔK_{TH} thresholds (compared with long crack results), and V-shaped da/dN–ΔK behavior for fatigue cracks extending less than 2 mm from the notch. Qualitatively, the transient short-crack behavior can be rationalized by considering that the grain-bridging zones for short cracks have yet to reach the steady-state size found for long cracks, where bridges are created and "exhausted" at an equal rate and the shielding contribution is essentially constant at a given applied driving force. As the load sustained by the smaller (short-crack) bridging zone is necessarily less than that of the steady-state zones, the short crack is likely to experience less shielding and hence a higher effective (near-tip) driving force at a fixed applied ΔK, leading to faster growth rates and lower fatigue thresholds. Similarly, the V-shaped crack-growth curve observed for short cracks can be explained by the fact that although the applied driving force is increasing with increasing crack length, the crack-tip shielding due to the grain bridges initially increases at a faster rate, causing the effective driving force at the crack tip to decrease; this leads to an initial reduction in crack-growth rates. After further crack growth, however, a steady state is reached and the growth rates match those of long cracks.

Such qualitative explanations have been used to rationalize short-crack effects for a wide range of materials;[16,21,22,57–59] however, there have been few reports of *quantitative* measurements of this reduced role of shielding to confirm this phenomenon for the fatigue of ceramics. Accordingly, the multi-cutting/crack-opening profile (MC/COP) and direct compliance (DC)[34] methods were used in the present work to quantify these effects.

(1) *MC/COP Method:* In Section V(2), K_0 was estimated to be 1.6 ± 0.2 MPa·m$^{1/2}$, and accordingly, assuming that at the fatigue threshold $K_{max,tip} = K_0$, an estimate can be made for the initiation condition for growth of short fatigue cracks with no grain

bridging. This corresponds to a fatigue threshold of $\Delta K_{eff,TH} = 1.4 \pm 0.2$ MPa·m$^{1/2}$ using the load ratio of $R = 0.1$ for the present study; this range is plotted in Fig. 11 along with the steady-state long-crack and short-crack data from various tests.

(2) *DC Method:* K_{br} values at different growth rates were computed using the standard C(T) stress-intensity solution[60] assuming P_{br}, determined as in Section III(3), is applied at the load line.[34] With knowledge of the bridging stress intensities, Eq. (2) was used to calculate the effective stress-intensity range, ΔK_{eff}. Such bridging-corrected estimates are plotted as a function of ΔK_{eff}, and are presented in Fig. 11.

It is apparent from Fig. 11 that when the long crack data are adjusted for crack bridging by characterizing the growth rates in terms of the effective (near-tip) driving force, the growth-rate curve and the value of the ΔK_{TH} threshold are shifted to lower values. While the DC method provides results in good agreement with the measured short-crack data taken from standard notched samples with $\Delta a_f > 100$ μm, the accuracy of this method is limited. Indeed, these computed ΔK_{eff} values exceed those measured for 20–60 μm cracks emanating from micronotches. Also, the DC method does not provide a unique solution for K_{br}; specifically, multiple bridging stress distributions with different associated values of K_{br} may result in the same value of P_{br} measured at the load line. Thus, the DC method is only a first approximation.

In contrast, the MC/COP method provides a worst-case threshold of $\Delta K_{eff,TH} = 1.4 \pm 0.2$ MPa·m$^{1/2}$ that corresponds well to data for the shortest measured cracks in this study grown from razor micronotchs, also shown in Fig. 11, which represent growth from ~20–60 μm at $\Delta K \approx 1.8$ MPa·m$^{1/2}$. Despite the limitations of these later experiments (e.g., crack front most likely discontinuous), it does serve to illustrate that crack growth is a concern at stress-intensity ranges below both the short-crack threshold measured for $a \geq 100$ μm and the effective threshold estimated by the DC method shown in Fig. 11. Accordingly, it is expected that the estimated effective threshold of $\Delta K_{eff,TH} = 1.4 \pm 0.2$ MPa·m$^{1/2}$ given by the MC/COP method is the most reasonable approximation of the worst-case short-crack behavior in the present AD995 alumina. Such results reaffirm the notion that crack size effects in fatigue may be attributed to a lack of grain bridging. Additionally, they demonstrate that for grain-bridging ceramics, the thresholds for crack initiation are low, much smaller than typical long-crack ΔK_{TH} values, in keeping with the necessarily weak grain boundaries. However, growth rates for short cracks can decay quickly, and more work is needed to provide a quantitative understanding of all short-crack behavior based on a comprehensive understanding of the evolution of the bridging zone under cyclic loading conditions.

(5) Estimating Other Short/Small Crack Behavior

In the present study, short-crack fatigue effects can be seen to occur over millimeter dimensions and are readily observed because of the slowly rising R-curve behavior of the AD995 alumina. Most ceramics of structural engineering interest, such as tough, self-reinforced silicon nitride and silicon carbide, however, have finer grain sizes and/or steeper R-curves that would be expected to limit such short-crack effects to much smaller crack dimensions than the 2 mm zones found in this present study. For example, no crack size effects were recognized for small ~200 μm surface cracks in a high-toughness SiC ceramic,[18,19] where the small, elongated grains (~5.5 μm in length, ~0.7 μm in diameter) resulted in far steeper R-curves, rising to a plateau toughness after crack extensions of only a few hundreds of micrometers, rather than many millimeters as in the current alumina. As those authors point out,[18,19] it is conceivable that smaller crack sizes may be necessary to observe such effects. While there are many experimental difficulties involved in conducting fatigue tests for very small (<200 μm) cracks, the present work indicates that by measuring the bridging contribution for long cracks, an effective worst-case short/small crack threshold can be approximated by conducting relatively simple long-crack growth experiments and
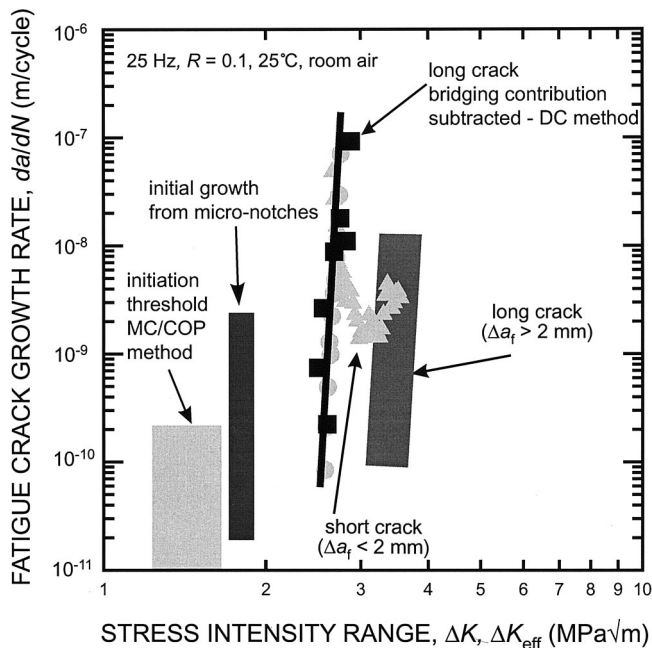
Fig. 11. Long-crack fatigue growth rates are plotted versus ΔK and versus ΔK_{eff} with the estimated contribution of grain bridging subtracted by the DC method and by the MC/COP method. When the bridging contribution is subtracted from the driving force for long-crack data by the more accurate MC/COP method, the results provide a lower value of ΔK (threshold) below which cracking has not been observed during any short-crack tests.

appropriately representing the results in terms of the near-tip, effective driving force. For the two methods used in the present work, although the DC method is simpler, it is nonconservative in its prediction of the effective fatigue threshold; in this regard, it is expected that the MC/COP method is more accurate in its prediction of the effective worst-case fatigue threshold in the absence of any bridging.

Finally, it should be noted that for very small cracks, additional non-steady-state effects on the growth rates may occur due to crack interactions with microstructural features on the same size scale, i.e., microstructurally small crack effects. Such cracks may sample local weak heterogeneities, giving rise to accelerated growth rates which the methods described in the present work would not take into account.

VI. Conclusions

Based on an experimental study that quantifies the role of grain bridging in influencing crack size effects in a commercial poly-crystalline alumina under both monotonic and cyclic loading conditions, the following conclusions can be made:

(1) From the multi-cutting compliance and crack-opening profile data, the intrinsic, near-tip, driving force necessary for crack advance in the present alumina was estimated to be $K_0 = 1.6 \pm 0.2$ MPa·m$^{1/2}$. This is proposed to correspond to the lowest point on the R-curve for very short cracks, and to the near-tip value of K_{max} achieved at the fatigue threshold.

(2) Short fatigue cracks in this alumina are demonstrated to have lower fatigue resistance, in the form of lower fatigue thresholds and higher growth rates at the same applied driving force, over the first 2 mm of growth, after which the rates merged with those of long cracks for growth rates below $\sim 10^{-8}$ m/cycle.

(3) Tests using different rates of change of ΔK verified that the steady-state growth behavior for long cracks occurred for the present alumina below $da/dN \approx 10^{-8}$ m/cycle, while at higher growth rates transient effects persist over more than 2 mm of growth which remain to be explored and understood.

(4) By initiating nearly bridge-free fatigue cracks from razor micronotches ($\rho \approx 15 \mu$m), crack growth was observed at the lowest driving forces found from any of the methods used in this study, $\Delta K = 1.7$ MPa·m$^{1/2}$.

(5) Transient short-crack fatigue behavior was attributed to the smaller degree of crack bridging due to the limited crack wake; indeed, the measured grain-bridging zone length for near-threshold, long fatigue cracks of ~ 2 mm corresponds well with the extension required for the convergence of the long- and short-crack fatigue growth rates. Additionally, when the contribution of grain bridging was quantitatively estimated and removed from the applied driving force (using the multi-cutting compliance and crack opening profile data), a worst-case fatigue threshold was determined in terms of the effective, near-tip, stress intensity to be $\Delta K_{eff,TH} = 1.4 \pm 0.2$ MPa·m$^{1/2}$, below which both long and short cracks were not observed to propagate.

(6) While short-crack fatigue behavior is difficult to measure directly in many grain-bridging ceramics where the bridging zones are much smaller than for this alumina (e.g., self-reinforced Si$_3$N$_4$, SiC), the present study demonstrates that reasonable estimates of lower-bound short-crack behavior may be obtained by quantifying the effects of grain bridging during standard long-crack fatigue experiments and presenting results in terms of the effective, near-tip, stress-intensity range. In this regard, the more rigorous, multi-cutting compliance/crack-opening profile technique is superior to the simpler direct compliance measurement method for quantifying the magnitude of such bridging.

Acknowledgments

References

[1]R. O. Ritchie and S. Suresh, "The Fracture Mechanics Similitude Concept: Questions Concerning Its Application to the Behavior of Short Fatigue Cracks," *Mater. Sci. Eng.*, **57** [2] L27–L30 (1983).

[2]J. Schijve, "Differences between the Growth of Small and Large Fatigue Cracks in Relation to Threshold K Values"; pp. 881–908 in *Fatigue Thresholds: Fundamentals and Engineering Applications*, Vol. 2. Edited by J. Backlund, A. F. Blom, and C. J. Beevers. Engineering Materials Advisory Services Ltd., Warley, U.K., 1982.

[3]S. Suresh and R. O. Ritchie, "Propagation of Short Fatigue Cracks," *Int. Met. Rev.*, **29** [6] 445–76 (1984).

[4]G. Vekinis, M. F. Ashby, and P. R. W. Beaumont, "R-Curve Behavior of Al$_2$O$_3$ Ceramics," *Acta Metall. Mater.*, **38** [6] 1151–62 (1990).

[5]P. L. Swanson, C. J. Fairbanks, B. R. Lawn, Y.-W. Mai, and B. J. Hockey, "Crack-Interface Grain Bridging as a Fracture Resistance Mechanism in Ceramics: I, Experimental Study on Alumina," *J. Am. Ceram. Soc.*, **70** [4] 279–89 (1987).

[6]R. W. Steinbrech, F. Deuerler, A. Reichl, and W. Schaarwächter, "Correlation of Crack Opening Displacement and Crack Resistance Curve of Alumina"; pp. 659–64 in *Science of Ceramics*, Vol. 14. Edited by D. Taylor, R. W. Davidge, R. Freer, and D. T. Livey. Institute of Ceramics, Shelton, Stoke-on Trent, U.K., 1987.

[7]R. Steinbrech, R. Knehans, and W. Schaawächter, "Increase of Crack Resistance during Slow Crack Growth in Al$_2$O$_3$ Bend Specimens," *J. Mater. Sci.*, **18**, 265–70 (1983).

[8]Y.-W. Mai and B. R. Lawn, "Crack-Interface Grain Bridging as a Fracture Resistance Mechanism in Ceramics: II, Theoretical Fracture Mechanics Model," *J. Am. Ceram. Soc.*, **70** [4] 289–94 (1987).

[9]C.-H. Hsueh and P. F. Becher, "Evaluation of Bridging Stress from R-Curve Behavior for Nontransforming Ceramics," *J. Am. Ceram. Soc.*, **71** [5] C-234–C-237 (1988).

[10]A. G. Evans and R. M. Cannon, "Toughening of Brittle Solids by Martensitic Transformations," *Acta Metall.*, **34** [5] 761–800 (1986).

[11]R. F. Cook, B. R. Lawn, and C. J. Fairbanks, "Microstructure–Strength Properties in Ceramics: I, Effect of Crack Size on Toughness," *J. Am. Ceram. Soc.*, **68** [11] 604–15 (1985).

[12]S. J. Burns and M. V. Swain, "Fracture Toughness of MgO-Partially-Stabilized ZrO$_2$ Specimens with K_R-Curve Behavior from Transformation Toughening," *J. Am. Ceram. Soc.*, **62** [3] 226–30 (1986).

[13]T. Fett, "Crack-Tip Toughness from Wide-Range COD Measurements," *Int. J. Fract.*, **114** [4] L29–32 (2002).

[14]J. Rödel, J. F. Kelly, and B. R. Lawn, "*In Situ* Measurements of Bridged Crack Interfaces in the Scanning Electron Microscope," *J. Am. Ceram. Soc.*, **73** [11] 3313–18 (1990).

[15]T. Fett, D. Munz, J. Seidel, M. Stech, and J. Rödel, "Correlation between Long and Short Crack R-Curves in Alumina Using the Crack Opening Displacement and Fracture Mechanical Weight Function Approach," *J. Am. Ceram. Soc.*, **79** [5] 1189–96 (1996).

[16]R. O. Ritchie and W. Yu, "Short Crack Effects in Fatigue: A Consequence of Crack Tip Shielding"; pp. 167–89 in *Small Fatigue Cracks*. Edited by R. O. Ritchie and J. Lankford. The Metallurgical Society, Warrendale, PA, 1986.

[17]R. O. Ritchie and J. Lankford, "Small Fatigue Cracks: A Statement of the Problem and Potential Solutions," *Mater. Sci. Eng.*, **A84**, 11–16 (1986).

[18]C. J. Gilbert, Y. S. Han, D. K. Kim, and R. O. Ritchie, "Small Crack Effects in Ceramic Materials"; pp. 283–88 in *Small Fatigue Cracks: Mechanics, Mechanisms, and Applications*. Edited by K. S. Ravichandran, R. O. Ritchie, and Y. Murakami. Elsevier, Oxford, U.K., 1999.

[19]C. J. Gilbert, Y. S. Han, D. K. Kim, and R. O. Ritchie, "Anomalous Cyclic Fatigue-Crack Propagation Behavior of Small Cracks in Monolithic, Grain Bridging Ceramics," *Ceram. Int.*, **26**, 721–25 (2000).

[20]R. H. Dauskardt, M. R. James, J. R. Porter, and R. O. Ritchie, "Cyclic Fatigue-Crack Growth in a SiC-Whisker-Reinforced Alumina Ceramic Composite: Long- and Small-Crack Behavior," *J. Am. Ceram. Soc.*, **75** [4] 759–71 (1992).

[21]J. Healy, A. J. Bushby, Y.-W. Mai, and A. K. Mukhopadhyay, "Cyclic Fatigue of Long and Short Cracks in Alumina," *J. Mater. Sci.*, **32**, 741–47 (1997).

[22]Y. H. Zhang and L. Edwards, "Small, Short, and Long Fatigue Crack Growth in an Advanced Silicon Nitride Ceramic Material," *Scr. Mater.*, **34** [10] 1561–66 (1996).

[23]F. G. Haubensak, A. Bhatnager, and R. H. Dauskardt, "Subcritical Growth of Microstructurally Small Cracks in Silicon Nitride Ceramics"; pp. 271–82 in *Small Fatigue Cracks: Mechanics, Mechanisms, and Applications*. Edited by K. S. Ravichandran, R. O. Ritchie, and Y. Murakami. Elsevier, Oxford, U.K., 1999.

[24]A. Ueno and H. Kishimoto, "Role of Grain Bridging Degradation of Small Crack on Propagation Behavior in Polycrystalline Alumina under Cyclic Load," *Mater. Sci. Res. Int.*, **4** [1] 26–32 (1998).

[25]Y. Mutoh, Y. Miyashita, and S. Zhu, "Small-Crack Behavior in Silicon Nitride at Elevated Temperature"; pp. 259–70 in *Small Fatigue Cracks: Mechanics, Mechanisms, and Applications*. Edited by K. S. Ravichandran, R. O. Ritchie, and Y. Murakami. Elsevier, Oxford, U.K., 1999.

[26]J. J. Kruzic, J. M. McNaney, R. M. Cannon, and R. O. Ritchie, "Effects of Plastic Constraint on the Cyclic and Static Fatigue Behavior of Metal/Ceramic Layered Structures," *Mech. Mater.*, **36** [1–2] 57–72 (2004).

[27]S. J. Bennison and B. R. Lawn, "Role of Interfacial Grain-Bridging Sliding Friction in the Crack-Resistance and Strength Properties of Nontransforming Ceramics," *Acta Metall.*, **37** [10] 2659–71 (1989).

[28]X. Hu and Y.-W. Mai, "Crack-Bridging Analysis for Alumina Ceramics under Monotonic and Cyclic Loading," *J. Am. Ceram. Soc.*, **75** [4] 848–53 (1992).

[29]S. Lathabai, J. Rödel, and B. Lawn, "Cyclic Fatigue from Frictional Degradation at Bridging Grains in Alumina," *J. Am. Ceram. Soc.*, **74** [6] 1348–60 (1991).

[30]R. D. Geraghty, J. C. Hay, and K. W. White, "Fatigue Degradation of the Crack Wake Zone in Monolithic Alumina," *Acta Mater.*, **47** [4] 1345–53 (1999).

[31]C. J. Gilbert, R. N. Petrany, R. O. Ritchie, R. H. Dauskardt, and R. W. Steinbrech, "Cyclic Fatigue in Monolithic Alumina: Mechanisms for Crack Advance Promoted by Frictional Wear of Grain Bridges," *J. Mater. Sci.*, **30** [3] 643–54 (1995).

[32]F. Guiu, M. Li, and M. J. Reece, "Role of Crack-Bridging Ligaments in the Cyclic Fatigue Behavior of Alumina," *J. Am. Ceram. Soc.*, **75** [11] 2976–84 (1992).

[33]R. H. Dauskardt, "A Frictional-Wear Mechanism for Fatigue-Crack Growth in Grain Bridging Ceramics," *Acta Metall. Mater.*, **41** [9] 2765–81 (1993).

[34]R. O. Ritchie, W. Yu, and R. J. Bucci, "Fatigue Crack Propagation in ARALL Laminates: Measurement of the Effect of Crack-Tip Shielding from Crack Bridging," *Eng. Fract. Mech.*, **32**, 361–77 (1989).

[35]H. F. Bueckner, "A Novel Principle for the Computation of Stress Intensity Factors," *Z. Angew. Math. Mech.*, **50** [9] 529–46 (1970).

[36]T. Fett and D. Munz, *Stress Intensity Factors and Weight Functions.* Computational Mechanics Publications, Southampton, U.K., 1997.

[37]F. H. Wittmann and X. Hu, "Fracture Process Zone in Cementitious Materials," *Int. J. Fract.*, **51** [1] 3–18 (1991).

[38]X.-Z. Hu and F. H. Wittmann, "Fracture Process Zone and K_r-Curve of Hardened Cement Paste and Mortar"; pp. 307–16 in *Fracture of Concrete and Rock: Recent Developments.* Edited by S. P. Shah, S. E. Swartz, and B. Barr. Elsevier, London, U.K., 1989.

[39]X. Hu and F. H. Wittmann, "Experimental Method to Determine Extension of Fracture-Process Zone," *J. Mater. Civ. Eng.*, **2** [1] 15–23 (1990).

[40]J. C. Hay and K. W. White, "Grain-Bridging Mechanisms in Monolithic Alumina and Spinel," *J. Am. Ceram. Soc.*, **76** [7] 1849–54 (1993).

[41]K. W. White and J. C. Hay, "Effect of Thermoelastic Anisotropy on the *R*-Curve Behavior of Monolithic Alumina," *J. Am. Ceram. Soc.*, **77** [9] 2283–88 (1994).

[42]C. J. Gilbert and R. O. Ritchie, "On the Quantification of Bridging Tractions during Subcritical Crack Growth under Monotonic and Cyclic Fatigue Loading in a Grain-Bridging Silicon Carbide Ceramic," *Acta Mater.*, **46** [2] 609–16 (1998).

[43]K.-S. Sohn, S. Lee, and S. Baik, "Analytical Modeling for Bridging Stress Function Involving Grain Size Distribution in a Polycrystalline Alumina," *J. Am. Ceram. Soc.*, **78** [5] 1401–405 (1995).

[44]W. F. Deans and C. E. Richards, "A Simple and Sensitive Method of Monitoring Crack and Load in Compact Fracture Mechanics Specimens Using Strain Gages," *J. Test. Eval.*, **7** [3] 147–54 (1979).

[45]N. E. Dowling, "Notched Member Fatigue Life Predictions Combining Crack Initiation and Propagation," *Fatigue Eng. Mater. Struct.*, **2**, 129–38 (1979).

[46]A. N. Palazotto and J. G. Mercer, "Crack Considerations in a Notched Compact Tension Specimen," *Eng. Fract. Mech.*, **37** [3] 473–92 (1990).

[47]T. Fett, C. Mattheck, and D. Munz, "On the Calculation of Crack Opening Displacement from the Stress Intensity Factor," *Eng. Fract. Mech.*, **27**, 697–715 (1987).

[48]R. Ballarini, S. P. Shah, and L. M. Keer, "Crack Growth in Cement-Based Composites," *Eng. Fract. Mech.*, **20** [3] 433–45 (1984).

[49]M. Wecharatana and S. P. Shah, "A Model for Predicting Fracture Resistance in Reinforced Concrete," *Cem. Concr. Res.*, **13**, 819–29 (1983).

[50]R. M. L. Foote, Y.-M. Mai, and B. Cotterell, "Crack Growth Resistance Curves in Strain-Softening Materials," *J. Mech. Phys. Sol.*, **34** [6] 593–607 (1986).

[51]C. J. Gilbert, J. J. Cao, W. J. MoberlyChan, L. C. De Jonghe, and R. O. Ritchie, "Cyclic Fatigue and Resistance-Curve Behavior of an *In Situ* Toughened Silicon Carbide with Al–B–C Additions," *Acta Metall. Mater.*, **44** [8] 3199–214 (1996).

[52]M. Iwasa and R. C. Bradt, "The Fracture Toughness of Single Crystal Alumina"; pp. 767–79 in Advances in Ceramics, Vol. 10, *Structure and Properties of MgO and Al_2O_3 Ceramics.* Edited by W. D. Kingery. American Ceramic Society, Columbus, OH, 1984.

[53]P. F. Becher, "Fracture-Strength Anisotropy of Sapphire," *J. Am. Ceram. Soc.*, **59** [1–2] 59–61 (1976).

[54]S. M. Wiederhorn, "Fracture of Sapphire," *J. Am. Ceram. Soc.*, **52** [9] 485–91 (1969).

[55]S. M. Wiederhorn, B. J. Hockey, and D. E. Roberts, "Effect of Temperature on the Fracture of Sapphire," *Philos. Mag.*, **28** [4] 783–96 (1973).

[56]J. J. Kruzic, R. A. Marks, M. Yoshiya, A. M. Glaeser, R. M. Cannon, and R. O. Ritchie, "Fracture and Fatigue Behavior at Ambient and Elevated Temperatures of Alumina Bonded with Copper/Niobium/Copper Interlayers," *J. Am. Ceram. Soc.*, **85** [10] 2531–41 (2002).

[57]J. J. Kruzic, J. P. Campbell, and R. O. Ritchie, "On the Fatigue Behavior of γ-Based Titanium Aluminides: Role of Small Cracks," *Acta Mater.*, **47** [3] 801–16 (1999).

[58]J. H. Andreasen, C. V. Moller, and B. L. Karihaloo, "Fatigue Crack Growth from Small Surface Cracks in Transformation-Toughened Ceramics," *J. Am. Ceram. Soc.*, **78** [2] 406–10 (1995).

[59]A. A. Steffen, R. H. Dauskardt, and R. O. Ritchie, "Cyclic Fatigue Life and Crack-Growth Behavior of Microstructurally Small Cracks in Magnesia-Partially-Stabilized Zirconia Ceramics," *J. Am. Ceram. Soc.*, **74** [6] 1259–68 (1991).

[60]Y. Murakami, *Stress Intensity Factors Handbook*, 1st ed. Pergamon Press, Elmsford, NY, 1987.   ☐